International Journal of Minerals, Metallurgy and Materials
Volume 30, Number 12, December 2023, Page 2459
https://doi.org/10.1007/s12613-023-2655-0

Insights into the oxidation resistance mechanism and tribological behaviors of multilayered TiSiN/CrV$_x$N hard coatings

Hongbo Ju[1,3)✉], *Moussa Athmani*[2)], *Jing Luan*[3)], *Abbas AL-Rjoub*[3)], *Albano Cavaleiro*[3,4)], *Talha Bin Yaqub*[4)], *Abdelouahad Chala*[2)], *Fabio Ferreira*[3)], *and Filipe Fernandes*[3,5)✉]

1) School of Materials Science and Engineering, Jiangsu University of Science and Technology, Zhenjiang 212003, China
2) Laboratory of Physics of Thin Films and Applications, University of Mohamed Khider, BP 145 RP, Biskra 07000, Algeria
3) CEMMPRE, ARISE, Department of Mechanical Engineering, University of Coimbra, Coimbra 3030-788, Portugal
4) IPN - LED & MAT - Instituto Pedro Nunes, Laboratory of Tests, Wear and Materials, Coimbra 3030-199, Portugal
5) ISEP, Polytechnic of Porto, Rua Dr. António Bernardino de Almeida, Porto 4249-015, Portugal
(Received: 23 February 2023; revised: 24 March 2023; accepted: 17 April 2023)

Abstract: In the last decades, vanadium alloyed coatings have been introduced as potential candidates for self-lubrication due to their perfect tribological properties. In this work, the influence of V incorporation on the wear performance and oxidation resistance of TiSiN/CrN film coatings deposited by direct current (DC) reactive magnetron sputtering is investigated. The results show that vanadium incorporation significantly decreases the oxidation resistance of the coatings. In general, two layers are formed during the oxidation process: i) Ti(V)O_2 on top, followed by a protective layer, which is subdivided into two layers, Cr_2O_3 and Si–O. ii) The diffusion of V controls the oxidation of V-containing coatings. The addition of vanadium improves the wear resistance of coatings, and the wear rate decreases with increasing V content in the coatings; however, the friction coefficient is independent of the chemical composition of the coatings. The wear of the V-containing coatings is driven by polishing wear.

Keywords: DC magnetron sputtering; TiSiN/CrV$_x$N multilayer coatings; oxidation resistance; tribology; wear rate

1. Introduction

Physical vapor deposition (PVD), chemical vapor deposition, and thermal spraying processes are some common surface modification techniques used in coating deposition [1–3]. In recent years, there has been considerable interest in the PVD technique, as it easily screens the chemical composition of the coatings and the deposition of more compact/dense coatings with improved mechanical, thermal, oxidation, corrosion, and tribological properties [4]. Transition metal nitrides produced by this technique have been widely applied as hard protective coatings in several industrial fields such as stamping, machining, aerospace, automotive, and other industrial sectors where components are used under severe conditions (high loading, corrosive environments, and high temperatures) [5–7]. Although the first binary nitride coatings (TiN and CrN) had somewhat succeeded for some decades in extending the service life of different components, including machining tools, currently, they have limited use due to the increasing solicitation conditions. TiN coatings exhibit excellent mechanical properties and thermal stability. Nevertheless, they tend to have a relatively elevated friction coefficient, and importantly, their resistance to oxidation is highly limited (onset point of oxidation of 500°C) [8–9]. The low oxidation resistance of this coating system has been attributed to the formation of a porous and nonprotective TiO_2 oxide scale on the top surface of the coating, which fails to prevent/block the diffusion of ions outward and O ions inward at high temperatures [9–10]. The limited oxidation resistance of TiN coatings renders them unsuitable for use in high-speed dry machining processes, where temperatures can reach up to 1000°C [10–11]. In contrast, the thermal stability of CrN films has been extensively studied [12–13]. Research has shown that CrN films undergo rapid oxidation upon exposure to temperatures exceeding 700°C, resulting in the formation of a Cr_2O_3 phase and a reduction of nitrogen in the films, thereby deteriorating its mechanical properties [14–16]. At high temperatures, Cr^{3+} diffuses outward to the film surface, while oxygen diffuses inward, creating a dense Cr_2O_3 layer. This oxide layer serves as an effective barrier, impeding the inward diffusion of oxygen [17]. In addition, the phase transformation from Cr_2N to CrN at elevated temperatures induces a porous and noncolumnar morphology of the Cr_2N coatings, resulting in poorer oxidation resistance compared to CrN coatings [18].

In the last decades, novel ternary, quaternary, and other coating systems deposited either as nanocomposite, monolayered, or multilayered architectures have been investigated

✉ Corresponding authors: Hongbo Ju E-mail: hju@uc.pt; Filipe Fernandes E-mail: fid@isep.ipp.pt

to extend the service life of components at high temperatures [19–20]. Many studies have shown that the addition of elements such as Si, Al, Mo, and Zr has yielded coatings with superior mechanical, thermal, oxidation, and tribological properties [21–25]. For example, the addition of Si to TiN can significantly affect their oxidation resistance [26–27]. Indeed, the formation of a continuous Si–O layer during the oxidation of those coatings limits the diffusion of the inward oxygen and outward metallic elements, thus improving the oxidation resistance [28–30]. Ternary Cr–Me–N coatings, where Me represents one of the alloying elements, have been investigated to enhance several properties of CrN coatings. V has been mainly used to improve the mechanical and tribological properties of the coatings. Aissani *et al.* [31] studied the effect of vanadium incorporation on the tribological properties of CrN coatings. The results showed that the friction coefficient decreases from 0.53 for CrN coating to 0.42 for CrN coating with 26% of V. Xu *et al.* [32] investigated the effect of vanadium incorporation on the tribological behavior of Cr–V–N coating. Authors reported that increasing the V amount slightly increases the average friction coefficient (COF) from 0.26 to 0.36 and the wear rate from 2.4×10^{-7} to 8.7×10^{-7} $mm^3 \cdot N^{-1} \cdot m^{-1}$. The hardness of coatings is not the only parameter controlling the friction property, and the surface roughness (R_a), along with the crystallinity, is also of great importance. Qiu *et al.* reported that alternating the CrN and VN coatings led to an increased hardness from 16.7 GPa for the CrN monolayer to 25 GPa for the CrN multilayer, and the corresponding friction coefficient decreased from 0.4 to 0.2 [33]. Fu *et al.* [34] studied the effect of current applied on the TiV target (70, 80, and 90 A) on the hardness, wear resistance, and corrosion resistance of the TiAlN/TiVN coating system. They reported that among the three coatings, the coating deposited by 90 A current exhibits the highest hardness, lower wear rate, and best corrosion resistance. However, following common problems were found in the works studying the influence of V addition on different coating systems: i) huge decrease in the onset temperature of oxidation and oxidation resistance of the coatings and ii) fast diffusion of V to the leading surface, after a critical time, to the total depletion of V from the entire volume of the coatings and consequently, to the deterioration of the tribological properties [35–37]. As highlighted in several studies, the challenge is to adequately control the V transport/diffusion to allow both low friction and wear over a long term and high oxidation resistance.

In our previous study, we proposed a coating design to control the V ion diffusion through a multilayered arrangement, altering high-oxidation-resistance TiSiN layers with VN layers [37]. The results showed that the increase in the TiSiN layer thickness on the multilayer architecture successfully improves the onset point of oxidation and oxidation resistance of coatings due to the formation of a more efficient and thicker Ti–Si–O layer. However, despite these results, the oxidation resistance of the coatings was still far from the temperatures needed for high-temperature applications (ranging from 700 to 1000°C). To improve the oxidation resistance of such coatings, their architecture was redesigned. The strategy was to replace the pure VN layer in the multilayer architecture with a high oxidation resistance layer (CrN) alloyed with different V concentrations. Thus, the study was focused on the influence of V addition on the morphology, structure, thermal stability, and onset point of oxidation of multilayered TiSiN/CrV_xN coatings [38]. The results showed that all deposited coatings exhibited a cubic B1 structure, irrespective of the chemical composition. Reportedly, all coatings exhibited a substoichiometric composition with the N concentration in the range of 47at%–48at%. The substoichiometry occurred in the Cr_xV_yN layer as Ti reacted more easily with nitrogen than with Cr, thereby causing less incorporation of N in the Cr-rich layer compared to the Ti-rich one. In addition, V alloying showed an insignificant effect on the adhesion resistance and the residual stress of multilayered TiSiN/CrV_xN coating. Dynamic oxidation results (heating from room temperature (RT) up to 1200°C at a constant rate of temperature increase of 20°C/min) showed that the onset point of oxidation was decreased from 850 to 750°C as soon as 2at% and 4at% of V were added to the reference multilayered TiSiN/Cr(V)N coating. 8at% of V reduced the onset temperature of oxidation of the coatings to 700°C. All dynamic oxidation curves also revealed that the oxidation resistance of coatings was degraded; however, those tests did not consider the oxidation kinetic and oxide scale growth, since a continuous changing of the kinetics diffusion occurred with temperature. In this investigation, isothermal oxidation tests were conducted to understand the oxide scale growth and kinetics of ion diffusion responsible for the degradation of the oxidation resistance of the multilayer TiSiN/Cr(V)N coatings. In addition, the effect of vanadium alloying on the tribological behavior at room temperature was also investigated.

2. Experimental

TiSiN/CrV_xN coatings, with different vanadium concentrations, were deposited on alumina (for oxidation resistance tests) and M2 steel (for wear tests) substrates by a direct current (DC) reactive magnetron sputtering machine operating in an unbalanced mode equipped with two rectangular (150 × 150 mm) Ti (99.9%) and Cr (99.9%) magnetron cathodes positioned at 90° in relation to each other (each target has 20 holes of 10-mm diameter). TiSiN was obtained by inserting seven pellets of silicon (ϕ10 mm) at the preferential erosion zone of the Ti target while the remaining holes were filled with Ti rods. However, V incorporation in the coatings was assessed by successively increasing the number of V pellets (ϕ10 mm) at the preferential erosion zone of the Cr target, i.e., 5, 10, and 20 pellets. A V-free TiSiN/CrN coating was deposited to serve as a reference coating. Substrates were ultrasonically cleaned in acetone and ethanol for 15 and 10 min, respectively. Then, they were mounted on a substrate holder, which can rotate around the center axis in front of the two targets. Before the deposition, the chamber was pumped to the pressure of 5×10^{-4} Pa. First, the samples were etched in Ar^+ ion bombardment for 30 min (under a pulsed bias of −270 V and pressure of 0.5 Pa). This was conducted

in parallel with the cleaning of the two targets by applying a power of 1.3 W/cm^2 for 15 min on each target. Then, TiSi adhesive and TiSiN gradient layers were deposited by applying a power of 5.3 W/cm^2 at the TiSi target with the substrate bias of −70 V. TiSi adhesive layer was produced at 0.5 Pa for 5 min using 22 sccm of Ar, and the TiSiN gradient layer was produced by rising the N flow progressively up to 80 sccm during 5 min with the corresponding total pressure. The rotation speed was maintained constant at 23 r/min. Subsequently, the main multilayer structure was produced by applying 7.0 W/cm^2 to the TiSi target and 5.3 W/cm^2 to the Cr target, using 17 sccm of Ar and 80 sccm of N, with a working gas pressure of 0.3 Pa under a pulsed bias of −70 V, and the substrate rotation speed was reduced to 1.5 r/min to produce multilayer coatings with a period thickness of ~60 nm. For all depositions, the deposition time was 60 min, and the deposition temperature was under 150°C. A summary of the deposition conditions, chemical composition, and the main properties of the coatings are summarized in Table 1 [38].

To investigate the effect of vanadium alloying on the isothermal oxidation resistance of the coatings, a thermogravimetric equipment (SETARAM Setsys Ev 1750, France)) was used. Isothermal oxidation tests were conducted in air for 2 h at 700, 900, and/or 1000°C depending on the chemical composition of the coatings, as summarized in Table 1 [38]. The sample weight gain was registered continuously during the test every 2 s using a microbalance with an accuracy of 0.01 mg.

Table 1. Chemical composition and the main properties of elaborated coatings [38]

Sample	Chemical composition / at%					Thickness / μm	Residual stress / GPa	Hardness / GPa	Young's modulus / GPa	Onset oxidation temperature / °C	Isothermal oxidation temperatures / °C
	N	Ti	Cr	Si	V						
C_0	47.8 ± 0.1	14.5 ± 0.2	34.0 ± 0.3	3.8 ± 0.1	0	3.3	−0.83	23 ± 3	306 ± 13	850	900/1000
C_2	47.1 ± 0.3	14.5 ± 0.2	32.4 ± 0.3	4.0 ± 0.1	2.1 ± 0.2	3.4	−0.72	28 ± 3	329 ± 14	750	900
C_4	47.9 ± 0.2	15.1 ± 0.3	28.9 ± 0.3	4.1 ± 0.1	4.1 ± 0.1	3.5	−0.67	28 ± 3	331 ± 15	750	900
C_8	47.9 ± 0.2	14.9 ± 0.3	24.8 ± 0.3	3.9 ± 0.1	8.4 ± 0.2	3.3	−0.74	31 ± 3	348 ± 17	700	700/900

After the oxidation, the surface and cross-sectional morphology of the oxidized coatings were characterized by scanning electron microscopy (SEM; ZEISS Merlin Gemini2, Germany), and the phases formed were characterized by XRD using a PANalytical X'Pert Pro diffractometer working in conventional mode. Spectra were acquired in the range of 20° to 70°.

Wear tests were conducted in a pin-on-disc equipment against Al_2O_3 balls. The samples and balls were sized 20 and 6 mm in diameter, respectively. The tests were performed by applying a normal load of 10 N, linear sliding speed of 0.1 m/s, duration of 15000 cycles, and relative humidity of 30%–40% at room temperature. During the wear tests, the variation in the friction coefficient vs. number of cycles was continuously recorded. A Mitutoyo SURFTEST SJ-500 profilometer was used to calculate the volume loss due to wear, and then Archard's law was applied to evaluate the specific wear rate [39]. To examine the obtained worn surfaces of the tested coating samples and the counterpart balls, two instruments were used: SEM and LEICA optical microscope. For the desired regions, chemical analyses were also conducted using the attached energy dispersive X-ray spectroscopy (EDS) to investigate the eventual chemical changes in the worn surfaces.

3. Results and discussion

3.1. Isothermal oxidation

The oxidation resistance of coatings strongly depends on their chemical composition and the isothermal temperature, as shown in Fig. 1. The reference TiSiN/CrN coating oxidized at 900°C exhibited an excellent oxidation resistance showing negligible oxidation weight gain, suggesting the formation of a protective oxide scales. At 1000°C, although the coating displayed a higher mass gain (0.06 mg/cm^2), the parabolic evolution of the curve still suggests the formation of a protective oxide scale. When 2at% and 4at% of V were added to the reference coating, the oxidation weight gain at 900°C increased to 0.09 and 0.17 mg/cm^2, respectively. The higher the V concentration on the coatings, the higher the oxidation weight gain, corroborating with the previous dynamic oxidation results [38], wherein a decrease in oxidation resistance was also noticed.

The C_8 coating with the highest vanadium content (8at%) was oxidized at two different temperatures of 700 and 900°C, respectively. The results showed that the isothermal oxida-

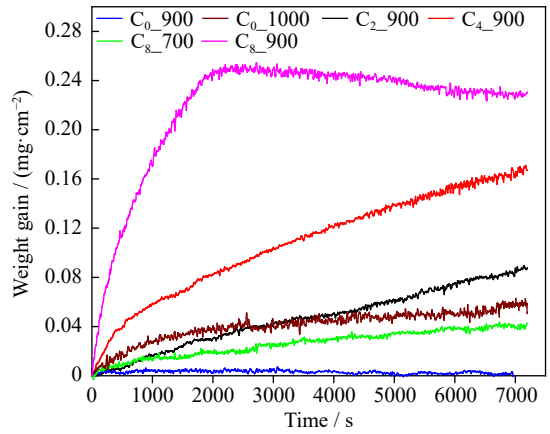

Fig. 1. Thermogravimetric isothermal analysis of coatings exposed at different temperatures for 2 h.

tion at 700°C also followed a parabolic law, suggesting that the diffusion of oxygen and metal cations is controlled by the formation of a protective layer. The mass gain at this temperature was lower than that for C_2 and C_4 coatings tested at 900°C, which agreed well with the lower kinetics of ion diffusion expected at this temperature. However, the oxidation of the C_8 coating at 900°C dramatically increased. The oxidation curve at this temperature displayed a strong increase in the mass gain, and then, a plateau was observed until the end of the experiment, indicating complete oxidation of the coating, as shown later.

Based on the isothermal oxidation curves, the higher the V concentration in the coatings, the lower the oxidation resistance. To further explore the composition and structure of the oxide scale, the as-produced coatings were characterized by XRD, SEM, and EDS.

The XRD diffractograms of the isothermal oxidized coatings are presented in Fig. 2. The oxide scale formed after oxidation of C_0 at 900°C was mainly composed of Cr_2O_3 (ICCD: 038-1479); however, a few weak peaks related to TiO_2 (ICCD: 076-0649) were revealed via XRD. According to the EDS elemental map distribution (Fig. 3) and elemental line profile (Fig. S1 in supplementary material) of C_0 oxidized at 900°C, the formed oxide scale is a mixture of TiO_2, Cr_2O_3,

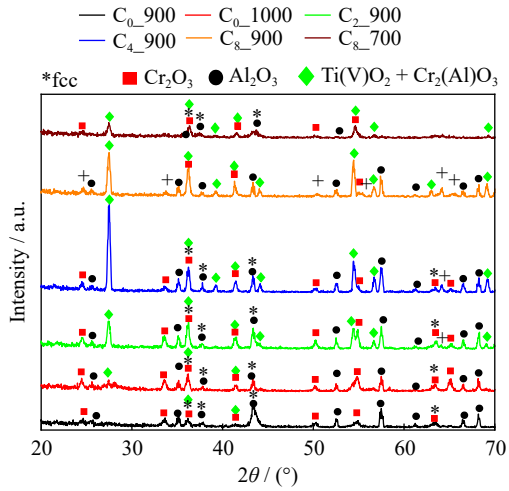

Fig. 2. XRD patterns of the coatings in grazing incidence mode after isothermal oxidation.

and Si–O phases. However, the coating oxidized at 1000°C exhibited two different oxide layers: a Ti–O rich layer corresponding to the TiO_2 phase on the top, followed by a mixture/compact layer mainly composed of Cr–O and Si–O oxides. Si–O could not be detected by XRD due to its amorphous character, which agrees well with the literature, where similar observation was reported [40–41].

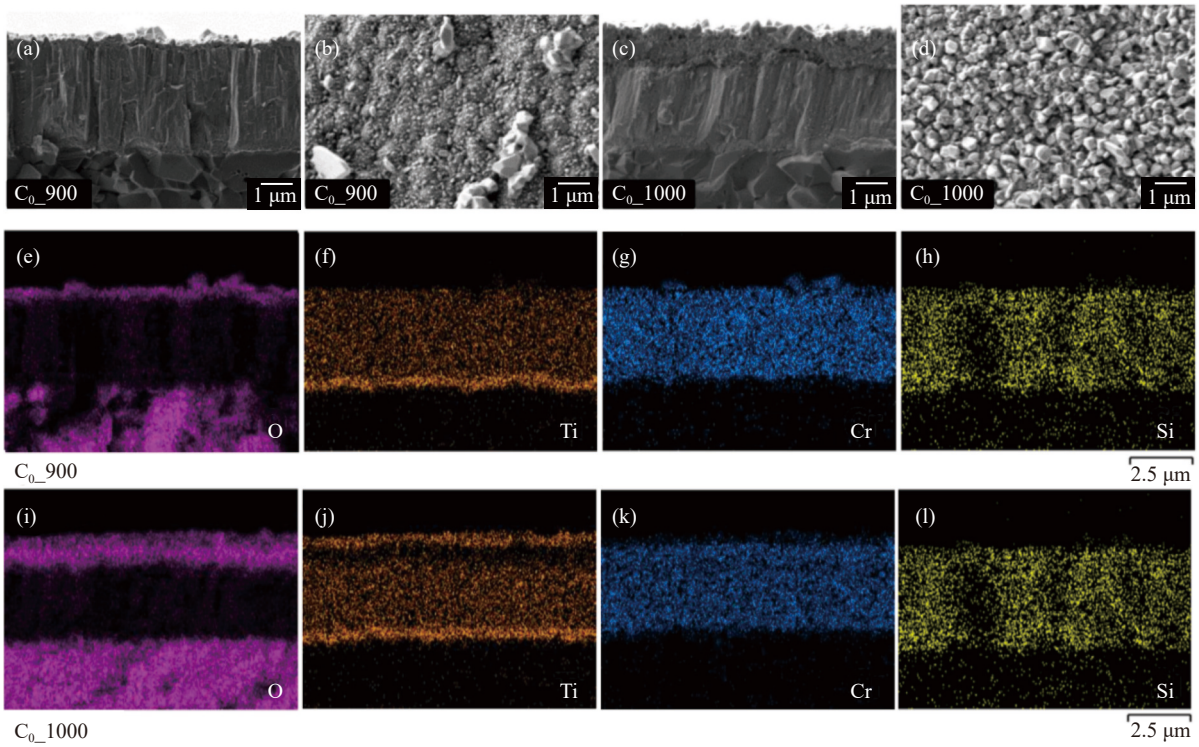

Fig. 3. Cross-section (a, c), surface morphology (b, d), and corresponding EDS elemental maps of C_0 oxidized at 900°C (e–h) and 1000°C (i–l).

Additionally, for both oxidation temperatures (900°C and 1000°C), the XRD analysis revealed peaks belonging to the remaining coating, confirming that the coating was not totally oxidized, corroborating well with the cross-sectional morphology presented in Fig. 3. Nevertheless, the entire surface of C_0 oxidized at 1000°C was covered with rutile (TiO_2) crystallites (Fig. 3). The elemental map of C_0 oxidized at 1000°C (Fig. 3) showed the formation of a titanium-depleted zone beneath the surface layer containing titanium oxides, possibly resulting from the migration of titanium to form oxides on the surface. Thus, titanium oxide displayed a higher growth rate than chromium and silicon oxide but was far less protective.

The high growth rate of titanium oxide further leads to cracks and pore formation. Moreover, reportedly, compact Cr_2O_3 and Si–O oxide scales are considered protective [29,42] and act as an efficient barrier to ion diffusion when their thickness is sufficient. Consequently, the coating is protected from further oxidation. However, the formation of TiO_2 is controlled by the inward diffusion of O^{2-} and the outward diffusion of Ti^{4+} through the formed protective layer. The signals of Al_2O_3 (Al_2O_3, ICCD: 046-1212) coming from the substrate were detected via XRD analysis.

Based on the SEM analysis of oxidized C_2, C_4, and C_8 at 900°C (Fig. 4), the addition of vanadium clearly significantly affects the oxidation resistance of coatings. Evidently, the thickness of the oxide scale formed on the coating surface increased with the increasing V content. The results confirmed that a small percentage of vanadium (2at%) is sufficient to disrupt the oxidation resistance of the coating, as suggested by the weight gain curves in Fig. 1, where the weight gain increases from 0.09 mg/cm^2 for C_2 to 0.25 mg/cm^2 for C_8 oxidized at 900°C. Cross-sectional morphology also showed incomplete oxidation of C_2 and C_4, while C_8 was fully oxidized, corroborating with the oxidation weight gain curves shown in Fig. 1.

As evident from the XRD analysis, two main products

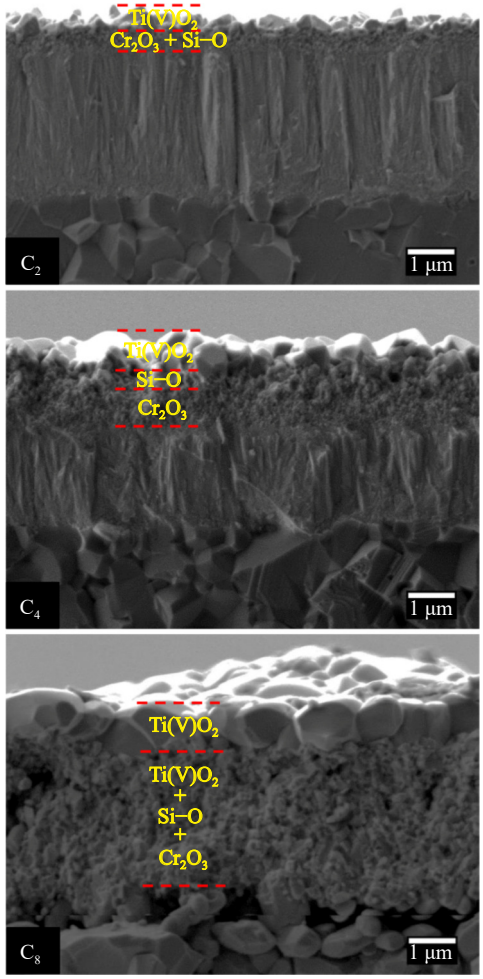

Fig. 4. Cross-sectional morphologies of C_2, C_4, and C_8 coatings after isothermal oxidation.

were formed during the isothermal oxidation of V-doped coatings: TiO_2 (ICCD: 076-0649) and Cr_2O_3 (ICCD: 038-1479). Similar to C_0, the signals of Al_2O_3 (ICCD: 046-1212) emanating from the substrate could be detected. Additionally, peaks belonging to the remaining coatings were detected via XRD for C_2 and C_4, confirming the results discussed above.

Based on the EDS elemental maps (Fig. 5) and elemental line distribution (Fig. S2 in supplementary material) of C_2, C_4, and C_8, the following results could be distinguished. i) Amorphous Si–O phase should exist for C_2, C_4, and C_8 similar to C_0 coating. ii) the oxide scale of C_2 oxidized at 900°C primarily consists of two oxide layers (Fig. 5(a) and Fig. S2(a) in supplementary material): on top Ti–O rich layer corresponding to TiO_2 followed by a second layer consisting of porous and/or discontinuous layer, which is divided into two sublayers, an intermediate Cr_2O_3 layer followed by Si–O layer; iii) increasing V to 4at% shows a slight modification on the distribution of oxides layers. As seen from Fig. 5(b) and Fig. S2(b), the formed oxide scale is mainly composed of three layers: (Ti,V)–O rich layer on top followed by the Si–O rich layer, and finally, a mixture of Cr–O and Si–O layer. The diffusion of vanadium to the surface is clearly visible by the increasing V signals in the near-surface region, giving rise to a V-depleted zone in the lower layers due to the outward diffusion of vanadium. The same type of oxides as identified for the C_2 coating could be indexed for the C_4 coating. However, the intensity of the TiO_2 diffraction peak positioned at 27.5° increases significantly, suggesting a thicker oxide scale. iv) Literature shows that it is possible that V–O formed during oxidation might dissolve into TiO_2, and knowing the high solubility of V with Ti, a $Ti(V)O_2$ phase with V in a solid solution could be formed [43]. This phase has already been reported to be formed in our previous work and on other oxidized TiN-based coatings containing V [35]. v) Due to the outward migration of Ti^{4+} ions to the surface during oxidation, a Ti-depleted zone is also observed, as shown in the elemental maps distribution. vi) The cross-sectional morphology of the coating with high V concentration displayed the formation of a highly open/porous microstructure. However, elemental map distribution (Fig. 5(c)) and XRD analysis reveal that the formed oxide scale is a mixture of all the products discussed above. Consequently, the higher the vanadium concentration, the higher the oxidation rate and the easier the disruption of the formation of the protective continuous oxide layers. This could be explained by the occupation of the sites of Ti^{4+} ions by V^{2+} and/or V^{3+} ions, the increase of defect concentrations (oxygen ion vacancies) in the TiO_2 phase that maintain the electroneutrality condition, and their increased speed relative to the growth of oxides. The substitution for Ti^{4+} with the valence of +4 by V ions with the valence of +2 or +3 decreases the electrons of $2e^-$ or $1e^-$ from the concentration of conduction electrons [43]. Similar results were found by Ref. [21], where the substitution of Ti^{4+} by V^{3+} ions in the TiO_2 lattice would increase the concentration of interstitial metallic Ti^{4+} ions and decrease the number of excess electrons, consequently increasing the oxidation rate.

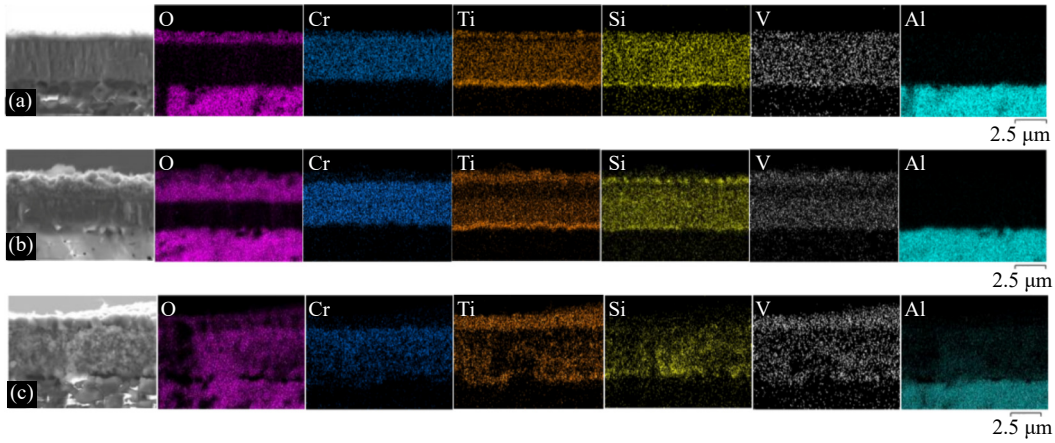

Fig. 5. SEM cross-sections and corresponding elemental maps of TiSiN/CrV$_x$N coatings oxidized at 900°C: (a) C$_2$; (b) C$_4$; (c) C$_8$.

Strong signals of Al were detected by the EDS analysis through the coating C$_8$, suggesting that Al diffuses out from the substrate through the coating. Based on the XRD analysis, a new phase of Cr_2O_3 with Al in solid solution (ICDD card: 084-0315) is indexed in the case of C$_2$, C$_4$,and C$_8$ [38].

Notably, this coating (C8) was tested at a lower temperature (700°C). SEM analysis showed that the coating is not totally oxidized (Fig. S3 and Fig. S4) and displays similar oxide scale as C$_2$ but with a good oxidation resistance translated by the lowest weight gain (0.04 mg/cm^2, Fig. 1). The oxide scale of C$_8$ oxidized at 700°C was typically composed of Ti(V)O_2 layer on the top surface followed by a layer composed of Cr_2O_3 and Si–O oxides.

3.2. Tribology

3.2.1. Friction coefficient

Literature reports that the friction coefficient is related to several parameters, such as applied loads, temperatures, and friction pair material [44–45]. Fig. 6 presents the friction coefficient of the coatings tested against Al_2O_3 balls at RT. The evolution of the friction coefficient is registered continuously as a function of the total number of cycles (15000 cycles). All friction curves present two stages: running-in and steady-state stages. The friction coefficient at the running-in stage increases steeply from the initial value of 0.2–0.6 in the first 400 cycles. The increase in the COF values is mainly due to the initial contact interaction and contact stresses of irregular asperities from both the film and ball. Then, the value decreases until the contact starts to adapt, establishing a stable wear mechanism and, consequently, a stable COF. The COF curve of the C$_0$ sample at the steady-state stage is relatively smooth and constant. However, when vanadium is added to the coatings, an oscillation of the friction coefficient curves is observed before reaching the steady state. This behavior may be attributed to the plastic deformation during the wear tests and the variation in the coating's roughness due to V incorporation [38]. After 12200 cycles, the COF curves became smooth and constant.

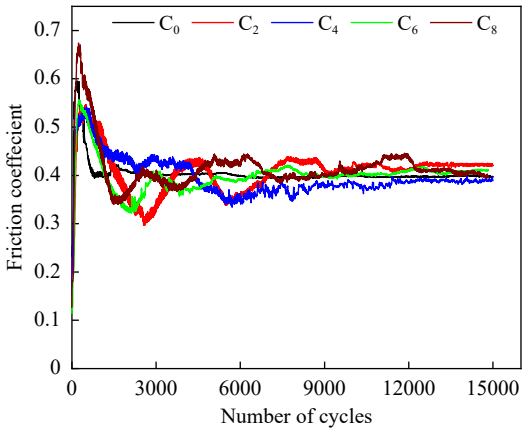

Fig. 6. Friction coefficient of coatings as a function of the number of cycles tested against Al_2O_3 balls at RT.

Conclusively, alloying the coating with vanadium does not affect the friction coefficient, and the values are in the range of 0.39–0.42, relatively lower than other V-containing coatings [5,45–46]. This result agrees well with the work of Qiu *et al.* [47], who studied the tribological behavior of CrVN/VN with different period thicknesses. The results showed that all multilayer coatings have a similar friction coefficient of around 0.23, considerably lower than CrVN and VN monolayers. Moreover, Rapoport *et al.* [48] reported that the presence of vanadium does not show any distinct influence on the friction coefficient evolution at RT when studying the CrV$_x$N monolayer. Yang *et al.* [45] studied the effect of periodic thickness on the mechanical and tribological properties of TiSiN/CrN. The results showed that COF decreases with periodic thickness. A similar value of COF 0.35–0.5 was obtained for the periodic thickness equal to 6.2 nm.

3.2.2. Wear rate

Fig. 7 shows the specific wear rate of the coatings and Al_2O_3 balls tested at RT, showing that the reference C$_0$ displays the highest wear rate of the coating, as well as the lowest one of the counterpart. With the increasing vanadium content in the coating system, an improvement in the wear rate is clearly observed for the coatings, and the wear rate of the ball increases in good agreement with the hardness trend presented in Table 1. Several studies have highlighted that the addition of V to Cr-based coatings in solid solution significantly improves their wear resistance [47,49]. From the 2D wear track profiles of the coatings shown in Fig. 8, with the increasing vanadium content, the wear tracks became shal-

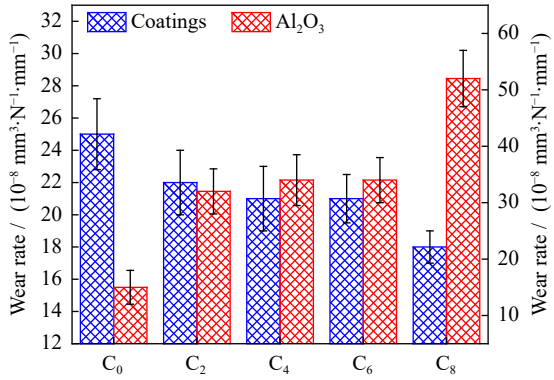

Fig. 7. Specific wear rate of the considered coatings (left *y*-axis) and Al_2O_3 balls (right *y*-axis).

low, indicating the positive effects of V alloying on the wear resistance of these coatings.

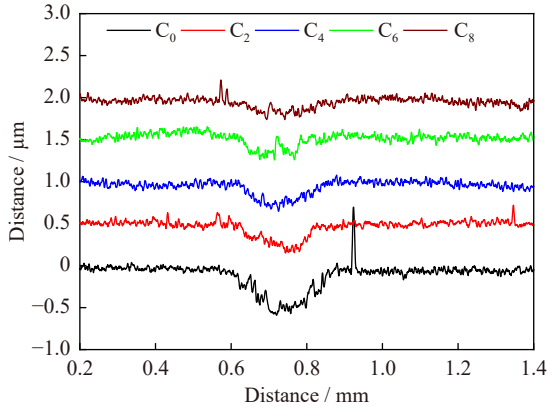

Fig. 8. 2D wear track profiles of the worn surfaces.

3.2.3. Wear mechanism

Fig. 9 shows the worn surfaces of C_0, C_4, and C_8 and their respective EDS analyses. The wear of the reference coating was governed by abrasion, wherein the formation of deep grooves on the wear track is evident. The grooves were formed due to the penetration of the hard Al_2O_3 balls into the coating, resulting in the removal of materials through micromachining. EDS point analysis performed on the wear tracks of the coating revealed no signals of O, suggesting the good oxidation resistance of the film as confirmed by the isothermal oxidation test. Moreover, no signals from the substrate were detected. In contrast, when the vanadium amount increased in the coating system (C_4 and C_8), the wear mechanism was completely changed into the polishing wear mechanism, as demonstrated by the smooth, worn surface (Fig. 9). The black, well-adhered, so-called fish-like debris was distributed through the wear track. EDS analysis performed on the fish-like wear debris revealed that they were mainly composed of O and V and traces of Ti, Cr, and Si, suggesting the formation of V–O, Ti–O, Cr–O, and Si–O oxide phases in small scales still insufficient in producing the V-oxide lubricious agent at RT. Notably, the EDS analysis showed that the other zones of the wear tracks were identical to the deposit coatings. Fish-like wear debris is formed due to the plastic deformation of the film induced by the ball sliding against the coating [50–51]. Due to the sliding of the counterpart on the coating, the asperities will be detached, producing free wear particles from either the film or the ball. The continuous sliding movement of the ball will drag the wear debris against the coating surface, giving rise to their oxidation and contributing to the continuous removal of the coating. Moreover, Al signals were detected corresponding to the material detached from the ball.

4. Conclusions

In this study, the influence of vanadium addition on the oxidation process and vanadium diffusion during the isothermal annealing of TiSiN/CrV_xN coatings deposited by DC reactive magnetron sputtering is investigated. The oxidation of the reference coating at 900 and 1000°C is controlled by the formation of a protective oxide layer. The oxide scale of this coating mainly consisted of two layers: TiO_2 on the top, followed by a continuous layer, subdivided into Cr_2O_3 and Si–O layers. The existence of vanadium cations with lower oxidation states in the TiO_2 scale during the oxidation of V-alloyed coatings is the main factor influencing the oxidation resistance and disrupts the formation of continuous protective oxides. A new phase related to $Cr_2(Al)O_3$ was detected because of the Al diffusion from the substrate toward the oxide scale.

The results from the wear resistance showed that adding vanadium to the TiSiN/CrN system does not affect the coefficient of friction, around 0.4; thus, V incorporation clearly enhances the wear resistance of the coatings due to the increase in hardness. Moreover, the wear of the reference coating is governed by abrasion, wherein the formation of deep grooves is observed on the wear track. However, when vanadium is added to the coatings, the wear is driven by polishing, and the black, well-adhered, so-called fish-like debris is detected. The EDS analysis performed on the debris reveals that the coatings are mainly composed of O and V and traces of Ti, Cr, and Si, suggesting the formation of a complex oxide phase.

Acknowledgements

This work was financially supported by the National Natural Science Foundation of China (Nos. 51801081 and 52171071) and national funds through FCT of Portugal – Fundação para a Ciência e a Tecnologia, under a scientific contract of 2021.04115, CEMMPRE – ref. "UIDB/00285/2020" and LA/P/0112/2020 projects, FEDER funds through the COMPETE program – Operational Program on Competitiveness Factors and by national funds through FCT – Foundation for Science and Technology, Outstanding University Young Teachers of "Qing Lan Project" of Jiangsu Province of China, Excellent Talents of "Shenlan Project" of Jiangsu University of Science and Technology of China. A part of this study was supported by the Directorate-General of Scientific Research and Technological Development (Algeria).

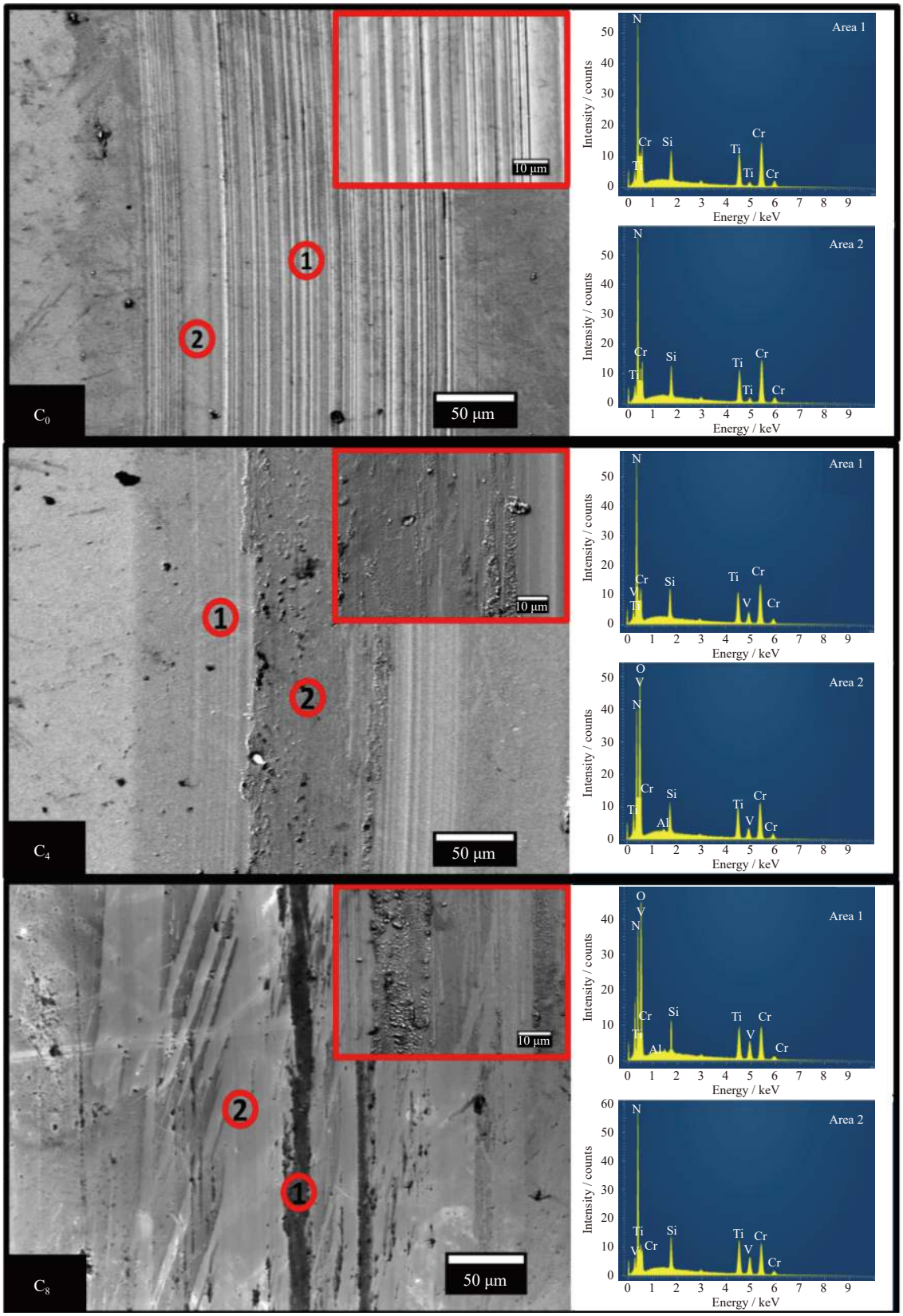

Fig. 9. SEM micrographs and the related EDS spectra of the wear tracks of C_0, C_4, and C_8 coatings tested at RT against the Al_2O_3 balls.

Conflict of Interest

Hongbo Ju is a youth editorial board member for this journal and was not involved in the editorial review or the decision to publish this article. The authors declare no conflict of interest.

Supplementary Information

The online version contains supplementary material available at https://doi.org/10.1007/s12613-023-2655-0.

Open access funding provided by FCT|FCCN (b-on).

References

[1] H.B. Ju, R. Zhou, J. Luan, *et al*., Tribological performance under different environments of Ti–C–N composite films for marine wear-resistant parts, *Int. J. Miner. Metall. Mater.*, 30(2023), No. 1, p. 144.

[2] V.Kh. Alimov and J. Roth, Deuterium retention in chemically vapor deposited tungsten carbide coatings and hot-rolled tungsten exposed to low-energy deuterium plasma, *Tungsten*, 4(2022), No. 1, p. 10.

[3] C. Wang, B.L. Ji, S.X. Gu, *et al*., Recent research progress on the compatibility of tritium breeders with structural materials and coatings in fusion reactors, *Tungsten*, 4(2022), No. 3, p. 170.

[4] H.B. Ju, D. Yu, J.H. Xu, *et al*., Crystal structure and tribological properties of ZrAlMoN composite films deposited by magnetron sputtering, *Mater. Chem. Phys.*, 230(2019), p. 347.

[5] H.B. Ju, D. Yu, L.H. Yu, *et al*., The influence of Ag contents on the microstructure, mechanical and tribological properties of ZrN–Ag films, *Vacuum*, 148(2018), p. 54.

[6] H.B. Ju, D.A. Yu, J.H. Xu, *et al*., Microstructure, mechanical, and tribological properties of niobium vanadium carbon nitride films, *J. Vac. Sci. Technol. A*, 36(2018), No. 3, art. No. 031511.

[7] H.B. Ju, N. Ding, J.H. Xu, *et al*., Improvement of tribological properties of niobium nitride films via copper addition, *Vacuum*, 158(2018), p. 1.

[8] Y.C. Chim, X.Z. Ding, X.T. Zeng, and S. Zhang, Oxidation resistance of TiN, CrN, TiAlN and CrAlN coatings deposited by lateral rotating cathode arc, *Thin Solid Films*, 517(2009), No. 17, p. 4845.

[9] Y.X. Xu, L. Chen, Z.Q. Liu, F. Pei, and Y. Du, Improving thermal stability of TiSiN nanocomposite coatings by multilayered epitaxial growth, *Surf. Coat. Technol.*, 321(2017), p. 180.

[10] W.H. Zhang and J.H. Hsieh, Tribological behavior of TiN and CrN coatings sliding against an epoxy molding compound, *Surf. Coat. Technol.*, 130(2000), No. 2-3, p. 240.

[11] I. Milošev, H.H. Strehblow, and B. Navinšek, XPS in the study of high-temperature oxidation of CrN and TiN hard coatings, *Surf. Coat. Technol.*, 74-75(1995), p. 897.

[12] M.A. Djouadi, C. Nouveau, O. Banakh, R. Sanjinés, F. Lévy, and G. Nouet, Stress profiles and thermal stability of Cr_xN_y films deposited by magnetron sputtering, *Surf. Coat. Technol.*, 151-152(2002), p. 510.

[13] C.K. Liu, H.B. Ju, P.X. Han, *et al*., The influence of carbon content on the microstructure, mechanical and frictional property of chromium carbon nitride composite films, *Vacuum*, 178(2020), art. No. 109368.

[14] L.Q. He, L. Chen, Y.X. Xu, and Y. Du, Thermal stability and oxidation resistance of $Cr_{1-x}Al_xN$ coatings with single phase cubic structure, *J. Vac. Sci. Technol. A*, 33(2015), No. 6, art. No. 061513.

[15] D.B. Lee, Y.C. Lee, and S.C. Kwon, High temperature oxidation of a CrN coating deposited on a steel substrate by ion plating, *Surf. Coat. Technol.*, 141(2001), No. 2-3, p. 227.

[16] F.H. Lu, H.Y. Chen, and C.H. Hung, Degradation of CrN films at high temperature under controlled atmosphere, *J. Vac. Sci. Technol. A*, 21(2003), No. 3, p. 671.

[17] A.E. Reiter, C. Mitterer, and B. Sartory, Oxidation of arc-evaporated $Al_{1-x}Cr_xN$ coatings, *J. Vac. Sci. Technol. A*, 25(2007), No. 4, p. 711.

[18] Z.B. Qi, B. Liu, Z.T. Wu, F.P. Zhu, Z.C. Wang, and C.H. Wu, A comparative study of the oxidation behavior of Cr_2N and CrN coatings, *Thin Solid Films*, 544(2013), p. 515.

[19] H.B. Ju, R. Wang, N. Ding, *et al*., Improvement on the oxidation resistance and tribological properties of molybdenum disulfide film by doping nitrogen, *Mater. Des.*, 186(2020), art. No. 108300.

[20] H.B. Ju, R. Zhou, J. Luan, *et al*., Multilayer Mo_2N-Ag/SiN_x films for demanding applications: Morphology, structure and temperature-cycling tribological properties, *Mater. Des.*, 223(2022), art. No. 111128.

[21] C.K. Liu, H.B. Ju, J.H. Xu, *et al*., Influence of copper on the compositions, microstructure and room and elevated temperature tribological properties of the molybdenum nitride film, *Surf. Coat. Technol.*, 395(2020), art. No. 125811.

[22] H.B. Ju, R. Zhou, S.J. Liu, L.H. Yu, J.H. Xu, and Y.X. Geng, Enhancement of the tribological behavior of self-lubricating nanocomposite Mo_2N/Cu films by adding the amorphous SiN_x, *Surf. Coat. Technol.*, 423(2021), art. No. 127565.

[23] H.B. Ju, R. Wang, W.X. Wang, J.H. Xu, L.H. Yu, and H. Luo, The microstructure and tribological properties of molybdenum and silicon nitride composite films, *Surf. Coat. Technol.*, 401(2020), art. No. 126238.

[24] Y.W. Lin, J.H. Huang, W.J. Cheng, and G.P. Yu, Effect of Ti interlayer on mechanical properties of TiZrN coatings on D2 steel, *Surf. Coat. Technol.*, 350(2018), p. 745.

[25] A. AL-Rjoub, L. Rebouta, N.F. Cunha, F. Fernandes, N.P. Barradas, and E. Alves, W/AlSiTiN_x/SiAlTiO_yN_x/SiAlO_x multilayered solar thermal selective absorber coating, *Sol. Energy*, 207(2020), p. 192.

[26] F. Vaz, L. Rebouta, P. Goudeau, *et al*., Characterisation of $Ti_{1-x}Si_xN_y$ nanocomposite films, *Surf. Coat. Technol.*, 133-134(2000), p. 307.

[27] H.B. Ju, L.Y. Xu, J. Luan, *et al*., Enhancement on the hardness and oxidation resistance property of TiN/Ag composite films for high temperature applications by addition of Si, *Vacuum*, 209(2023), art. No. 111752.

[28] M. Diserens, J. Patscheider, and F. Lévy, Mechanical properties and oxidation resistance of nanocomposite TiN–SiN_x physical-vapor-deposited thin films, *Surf. Coat. Technol.*, 120-121(1999), p. 158.

[29] J.B. Choi, K. Cho, M.H. Lee, and K.H. Kim, Effects of Si content and free Si on oxidation behavior of Ti–Si–N coating layers, *Thin Solid Films*, 447-448(2004), p. 365.

[30] L.C. Chang, M.C. Sung, Y.I. Chen, and C.H. Tseng, Mechanical properties and oxidation behavior of CrWSiN films, *Surf. Coat. Technol.*, 437(2022), art. No. 128368.

[31] L. Aissani, M. Fellah, and C. Nouveau, Structural mechanical

and tribological behavior of reactive sputtered Cr–N and Cr–V–N films, *Diffusion Found.*, 18(2018), p. 27.
[32] B.B. Xu, P. Guo, Z.Y. Wang, *et al*., Anti-wear Cr–V–N coating via V solid solution: Microstructure, mechanical and tribological properties, *Surf. Coat. Technol.*, 397(2020), art. No. 126048.
[33] Y.X. Qiu, S. Zhang, B. Li, *et al*., Improvement of tribological performance of CrN coating via multilayering with VN, *Surf. Coat. Technol.*, 231(2013), p. 357.
[34] F.X. Fu, S.W. Han, and Z. Chen, Influence of cathode current on corrosion resistance and tribological properties of TiAlN/TiVN hard coatings, *Ferroelectrics*, 549(2019), No. 1, p. 227.
[35] F. Fernandes, A. Loureiro, T. Polcar, and A. Cavaleiro, The effect of increasing V content on the structure, mechanical properties and oxidation resistance of Ti–Si–V–N films deposited by DC reactive magnetron sputtering, *Appl. Surf. Sci.*, 289(2014), p. 114.
[36] D.B. Lewis, S. Creasey, Z. Zhou, *et al*., The effect of (Ti+Al): V ratio on the structure and oxidation behaviour of TiAlN/VN nano-scale multilayer coatings, *Surf. Coat. Technol.*, 177-178(2004), p. 252.
[37] A. Al-Rjoub, A. Cavaleiro, and F. Fernandes, Structure, morphology, thermal stability and oxidation resistance of multilayered TiSiN/VN films: Influence of TiSiN-layer thickness, *J. Mater. Eng. Perform.*, 30(2021), No. 6, p. 3934.
[38] M. Athmani, A. AL-Rjoub, D. Cavaleiro, A. Chala, A. Cavaleiro, and F. Fernandes, Microstructural, mechanical, thermal stability and oxidation behavior of TiSiN/CrV_xN multilayer coatings deposited by D.C. reactive magnetron sputtering, *Surf. Coat. Technol.*, 405(2021), art. No. 126593.
[39] H.B. Ju, N. Ding, J.H. Xu, *et al*., The influence of crystal structure and the enhancement of mechanical and frictional properties of titanium nitride film by addition of ruthenium, *Appl. Surf. Sci.*, 489(2019), p. 247.
[40] T. Kacsich, S. Gasser, Y. Tsuji, A. Dommann, and M.A. Nicolet, Wet oxidation of $Ti_{34}Si_{23}N_{43}$, *J. Appl. Phys.*, 85(1999), No. 3, p. 1871.
[41] T. Kacsich and M.A. Nicolet, Moving species in $Ti_{34}Si_{23}N_{43}$ oxidation, *Thin Solid Films*, 349(1999), No. 1-2, p. 1.
[42] M. Danek, F. Fernandes, A. Cavaleiro, and T. Polcar, Influence of Cr additions on the structure and oxidation resistance of multilayered TiAlCrN films, *Surf. Coat. Technol.*, 313(2017), p. 158.
[43] T. Takahashi, Y. Minamino, H. Hirasawa, and T. Ouchi, High-temperature oxidation and its kinetics study of Ti–Al and Ti–V alloys in air, *Mater. Trans.*, 55(2014), No. 2, p. 290.
[44] R. Zhou, H.B. Ju, S.J. Liu, *et al*., The influences of Ag content on the friction and wear properties of TiCN–Ag films, *Vacuum*, 196(2022), art. No. 110719.
[45] S. Yang, Y. Chang, D. Lin, D. Wang, and W. Wu, Mechanical and tribological properties of multilayered TiSiN/CrN coatings synthesized by a cathodic arc deposition process, *Surf. Coat. Technol.*, 202(2008), p. 2176.
[46] P.H. Mayrhofer, P.E. Hovsepian, C. Mitterer, and W.D. Münz, Calorimetric evidence for frictional self-adaptation of TiAlN/VN superlattice coatings, *Surf. Coat. Technol.*, 177-178(2004), p. 341.
[47] Y.X. Qiu, B. Li, J.W. Lee, and D.L. Zhao, Self-lubricating CrVN coating strengthened via multilayering with VN, *J. Iron Steel Res. Int.*, 21(2014), No. 5, p. 545.
[48] L. Rapoport, A. Moshkovich, V. Perfilyev, *et al*., High temperature friction behavior of CrV_xN coatings, *Surf. Coat. Technol.*, 238(2014), p. 207.
[49] L. Aissani, M. Fellah, L. Radjehi, C. Nouveau, A. Montagne, and A. Alhussein, Effect of annealing treatment on the microstructure, mechanical and tribological properties of chromium carbonitride coatings, *Surf. Coat. Technol.*, 359(2019), p. 403.
[50] H.B. Ju, N. Ding, J.H. Xu, L.H. Yu, Y.X. Geng, and F. Ahmed, The tribological behavior of niobium nitride and silver composite films at elevated testing temperatures, *Mater. Chem. Phys.*, 237(2019), art. No. 121840.
[51] H.B. Ju, K.H. Huang, J. Luan, Y.X. Geng, J.F. Yang, and J.H. Xu. Evaluation under temperature cycling of the tribological properties of the Ag-SiN*x* films for green tribological applications, *Ceram. Int.*, 49(2023), No. 18, p. 30115.